Bioinsp. Biomim. **3** (2008) 046001 (10pp) doi:10.1088/1748-3182/3/4/046001

Mechanics of a mosquito bite with applications to microneedle design

M K Ramasubramanian, O M Barham and V Swaminathan

Department of Mechanical and Aerospace Engineering, North Carolina State University, Raleigh, NC 27695-7910, USA

E-mail: rammk@ncsu.edu

Received 6 September 2007
Accepted for publication 29 July 2008
Published 8 September 2008
Online at stacks.iop.org/BB/3/046001

Abstract

The mechanics of a fascicle insertion into the skin by a mosquito of the type *aedes aegypti* has been studied experimentally using high-speed video (HSV) imaging, and analytically using a mathematical model. The fascicle is a polymeric microneedle composed of a ductile material, chitin. It has been proposed that the mosquito applies a non-conservative follower force component in addition to the Euler compressive load in order to prevent buckling and penetrate the skin. In addition, the protective sheath surrounding the fascicle (labium) provides lateral support during insertion. The mechanics model presented approximates the fascicle as a slender column supported on an elastic foundation (labium) subjected to non-conservative (Beck) and conservative Euler loads simultaneously at the end. Results show that the lateral support of the fascicle provided by the labium is essential for successful penetration by increasing the critical buckling load by a factor of 5. The non-conservative follower force application increases the buckling load by an additional 20% and may or may not be necessary for successful penetration. Experimental results showing the importance of the labium have been cited to validate the model predictions, in addition to the video observations presented in this work. This understanding may be useful in designing painless needle insertion systems as opposed to miniaturized hypodermic needles.

M This article features online multimedia enhancements

1. Introduction

Puncturing of the human skin with a hollow needle is perhaps the most common invasive medical procedure to inject fluids into or extract fluids from the human body. Regardless of the size of the needle, unless an anesthetic is used, it is at least uncomfortable if not painful. During the past few years, considerable effort has been put into developing microneedles to replace the traditional hypodermic needle [1–4]. Microneedles are sharp hypodermic needles that are intended to be minimally invasive while accomplishing the task of penetrating the skin's outermost non-innervated layer to draw small volumes of blood or inject small quantities of therapeutic agents into the capillary-rich dermis layer, painlessly. It has been reported that a penetration up to 1.5 mm can be painless [5]. Typical sizes of these microneedles are 40–100 μm in diameter with sub-micron in tip radii. For comparison, the smallest hypodermic needle typically used (30 gage) is about 320 μm in outer diameter and 160 μm in inner diameter. Some microneedles are hollow, while some are solid with the therapeutic agents coated on the surface that dissolves once the needle is in the blood stream [6].

1.1. Microneedles

Using silicon micromachining technology, several microneedles and arrays of microneedles have been built [7, 8]. Henry *et al* [3] fabricated solid conical microneedle arrays with needle length 0.15 mm, 80 μm diameter at the base and a tip radius of 1 μm. These needles have been shown to penetrate painlessly into the stratum corneum (the external tough layer) of the skin and access the epidermis layer. Silicon-processed microneedles are not very tall (typically less than 0.50 mm) and brittle. A serrated silicon microneedle

(1 mm long, roughly 40 μm in diameter and a wall thickness of 1.6 μm), inspired by the anatomy of a mosquito, has been fabricated and tested by Oka *et al* [4]. They concluded that a force of 14.7 mN is sufficient to penetrate the skin while the silicon microneedle they fabricated had a strength of 58.8 mN in compression. The needle underwent a brittle fracture upon insertion. Brittle fracture can be a problem in live tissue; small fragments of silicon could be carried away in the blood stream, possibly lodging themselves in vital organs. Gattiker *et al* [9] described a hollow silicon microneedle with a height of 0.45 mm, a base length of 0.3 mm, a base width of 0.1 mm, hole diameter of 50 μm and an orifice aperture range between 300 and 375 μm above the base, and called it the e-mosquito. They claimed that a hole diameter of 50 μm is sufficient to draw blood without external pumps or suction devices. No experimental results were presented in the paper. Furthermore, the name e-mosquito was simply used to indicate that it is a microneedle penetration concept; penetration mechanics were not studied.

Oki *et al* [1] developed a hardened stainless steel microneedle, 100 μm outer diameter, 50 μm inner diameter and 0.6 mm in length. The tip was chemi-mechanically polished to a bevel of 10°. This needle was claimed to be painless by the researchers. A titanium microneedle was developed to mimic the mosquito fascicle dimensions and tested [10]. Blood extraction was possible at a rate of 2 μl min^{-1} for whole blood. They measured the indentation load for a 100 μm diameter needle to be 100 mN.

Polymeric solid microneedle arrays made with polycarbonate have been fabricated by an in-plane process and the needles were reconfigured in the out of plane mode, thereby making high aspect ratios possible [11]. The needle had a square cross section of 100 μm side. The height of the fabricated needles ranged from 0.5 to 1.5 mm, and the distance between the needles was 0.5 to 2 mm. The radii of curvature are approximately 2 μm, while the tip angles are in the range of 39–56°. Penetration tests were carried out to show that the needle array does penetrate the rat skin in the test. It is not clear whether the 100 μm $\times$ 100 μm square cross-section ending like a chisel will be painless in live tissue.

1.2. Mechanics of penetration

Despite the advances in microneedle fabrication and experiments with infusion into the skin [12], limited work has been done to understand the mechanics of penetration into the skin. Yang and Zahn [13] claim that a mosquito uses vibratory cutting at a frequency of 200–400 Hz, but no reference is provided. They state that current designs of needles do not tolerate forces associated with insertion and intact removal and are typically either too fragile or too ductile. Vibratory techniques are proposed as a method for inserting the needle into the skin. A silicon microneedle (100 μm diameter and 6 mm long) was used in their experiments. They show that there is a greater than 70% decrease in insertion force when the needle is vibrated compared to quasi-static insertion. The vibration applied was parallel to the skin surface and had an amplitude of 0.6 mm, vibrating in the kHz range. The static peak insertion force was found to be 300 mN; upon inserting the needle with vibration, the force drops to 50 mN.

Newton *et al* [14] discussed driving a microneedle array into the skin and reported that the use of ultrasonic vibration of the needle patch reduces the insertion force and provides better control of the penetration distance. For solid needles, the penetration force was reduced from 500 mN to 300 mN when the needle vibrated at ultrasonic frequencies (frequency not disclosed) and the penetration distance decreased from 0.3 mm to 0.18 mm.

A mechanical insertion study was done by Davis *et al* [15] to measure the insertion force versus displacement for 0.72 mm long, 30–80 μm tip radius and 5–58 μm wall thickness microneedles. They concluded that the insertion force ranged from 100 mN to 3000 mN, for the range of tip radii considered. Compressive strength of the needle was measured to be about 4000 mN. It was concluded that the needle will penetrate the skin without failing; however, the geometry of the needle was wider at the root tapering to a smaller diameter at the tip. The needle was also flat cut without a bevel. These idealizations prevent the needle from buckling and the only mode of failure is compressive crushing by fracture, but the needle may not be painless.

Roxhed *et al* [34] described an ultra sharp needle with tip radius less than 0.1 μm and results from a skin penetration study comparing the force required to penetrate the skin. They compared their results with needles from the published literature [8, 15]. Using a load cell and electrical conductivity measurements to determine penetration accurately, the penetration force was reported to be 10 mN compared to a minimum of 100 mN measured by Davis *et al* [15].

In summary, the general trend in microneedle technology has been to mimic the current hypodermic needle geometry and miniaturize it using a silicon micromachining process and other novel approaches for metal and polymeric materials. Decreasing the size and wall thickness increases the need for high stiffness materials. Silicon microneedles, although they are stiff enough to penetrate the skin, are brittle and fail inside the skin. Polymeric needles, on the other hand, have high toughness, but are not stiff enough to penetrate without buckling at the same size scale required for painless insertion.

However, in nature, we encounter the ultimate painless blood drawing device, namely, the mosquito fascicle. A female mosquito has evolved to penetrate the skin with a flexible biological (polymeric) needle that is extremely small and flexible, inserting it into the skin, drawing a full blood meal and leaving the host. The sucking of the fluid is done through a mouth part known as the proboscis. The anatomy of a mosquito is presented in great detail in [16]. The dimensions of an *aedes aegypti* fascicle are typically 1.8 mm long and 11 μm internal radius [17]. The typical blood meal volume is 4.2 mL [17] or 0.0275 mN [18], and the average feeding time is 141 s. In a study to understand the penetration, a mouse ear was monitored during the insertion process and the act of saliva secretion was identified [19]. The itching that is realized is due to the allergic reaction to the saliva that the mosquito secretes during the blood draw to prevent platelet aggregation and location of the blood vessels by

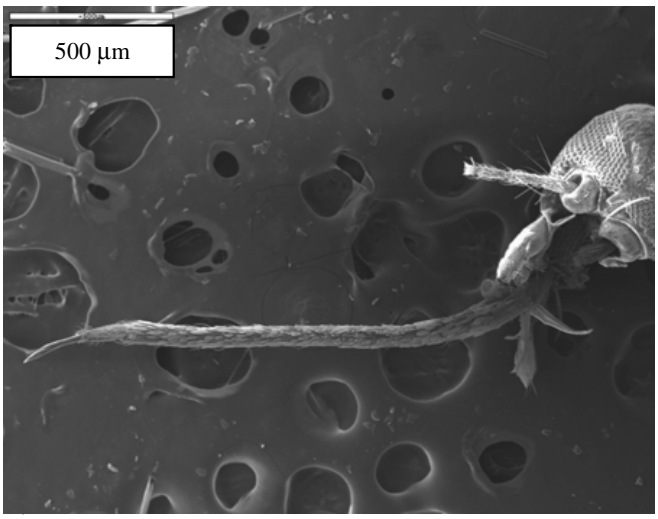

Figure 1. Mosquito head and proboscis.

promoting hematoma formation [20]. The probing process and subsequent insertion is studied in a descriptive fashion without mechanistically describing the underlying physics. The feeding behavior of mosquitoes has been described by Jones [18]. The feeding apparatus is described as something much beyond a hypodermic needle, but rather an exquisitely made piece of biological machinery, sawing its way through the skin. However, the mechanics aspects of feeding were not addressed.

In this study, we have made observations of how a mosquito uses its fascicle and penetrates the skin painlessly. A mathematical model for the behavior of a mosquito fascicle under axial load has been modeled. Based on the results, microneedle designs that can be polymeric, small and can penetrate the skin can be developed.

2. Experimental observations

2.1. Mosquito anatomy

The mosquito feeds through a tubular structure known as the proboscis. The proboscis extends from the mouth and projects in front like the trunk of an elephant. The proboscis is the name for a collective structure that consists of the outer sheath known as the labium, and a bunch of feeding stylets, known as the fascicle. The fascicle consists of a labrum tube which is the primary path for blood flow; mandibles which are also thin tubes, maxilla with saw toothed tips and a flat hypopharynx with a central salivary duct [18]. In the present work, the mosquito head and mouth parts were observed using a scanning electron microscope (SEM) in order to analyze the anatomy from a mechanics point of view [21]. Figure 1 shows a SEM picture of the mosquito head, with the proboscis covered by the outer sheath (labium) with a hair-like structure at the tip, called the labella. The fascicle tip is shown protruding from the end of the labium. Figure 2 shows a close-up of the tip. Normally, the fascicle is fully withdrawn into the labium. The proboscis is about 1.5 to 2.0 mm in length. The inner diameter of the labium is about 40 μm, and the

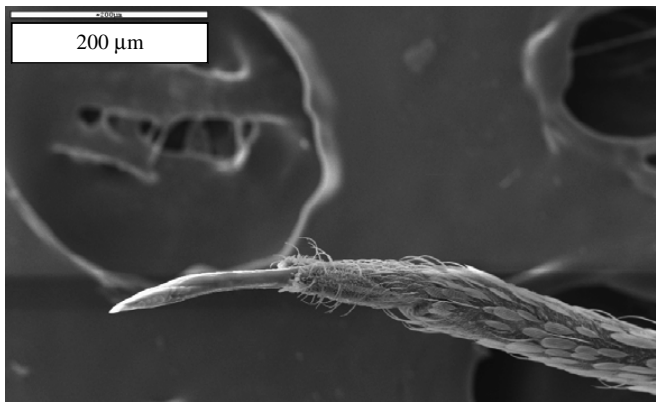

Figure 2. Fascicle tip with labella retracted.

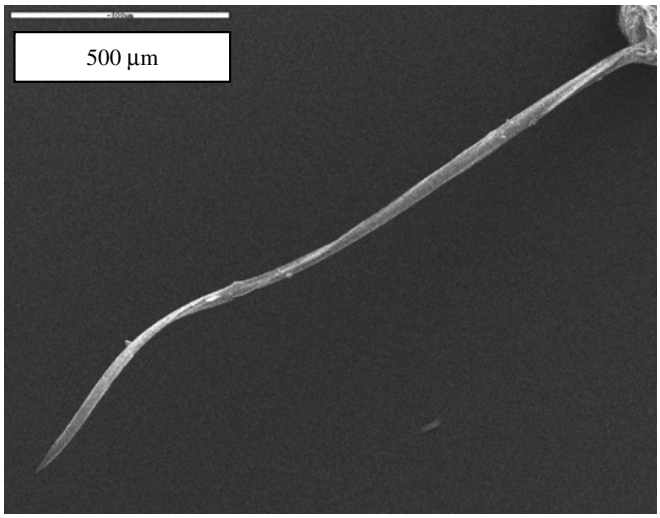

Figure 3. Desheathed fascicle.

inner diameter of the fascicle is about 20 μm. The curvature at the tip seen in figures 1 and 2 is attributed as an artifact of the peeling process and the drying of the fascicle under the SEM. Figure 3 shows the fascicle completely removed from the labium. The picture shows clearly the long slender nature of the fascicle with a sharp tip. The tip itself is shown in figure 4.

The tip of the fascicle is very sharp, tapering from about 10 μm to less than 1 μm over the last 50 μm of the fascicle. Further, the tip appears to have a V-shaped ridge near the tip over the last 50 μm of length. Ridges in thin sheet-like structures, especially sheet metal, are well known to provide additional stiffness and reinforcement [31]. The tip almost has a remarkable resemblance to a hypodermic needle, but is much smaller in size and flexible.

2.2. Mosquito skin piercing behavior

Mosquito feeding process was filmed using a high-speed video (HSV) camera (Fastcam-APX 120K, manufactured by Photron USA, San Diego, CA). This camera is capable of filming 2000 full frames per second (fps). 2000 fps filming speed was used for high magnification observation of the mosquito fascicle penetration process, while 250 fps speed was used to observe the probing behavior. This reduction in fps enabled filming

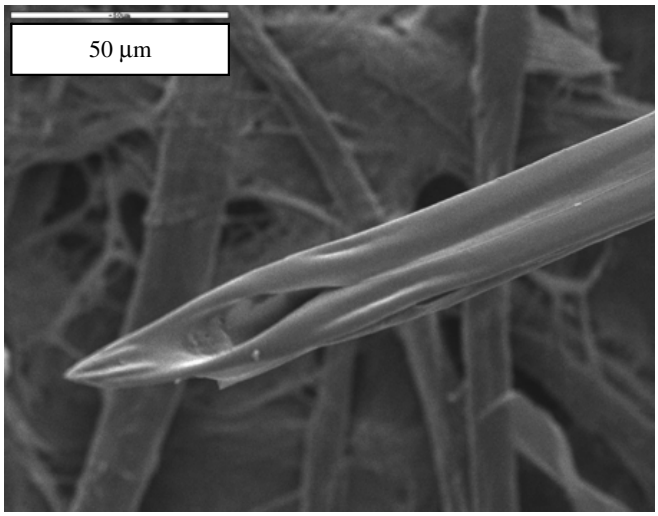

Figure 4. Fascicle tip.

for a longer period of time so that the probing at different sites could be captured. An abridged version of the video clip is available from the online version of this journal.

From the video, the following observations can be made.

- The mosquito lands on the host and starts thrusting the proboscis onto the skin.
- If the angle of impact, head orientation, and the applied force are not suitable for continued penetration, the proboscis starts to bend instead of penetrating into the skin. This is shown in figure 5(*A*).
- The mosquito pulls back and probes other spots until a suitable spot is found where it is able to push down its proboscis without bending. At this point, the fascicle tip anchors down into the top layer of the skin. The frequency of probing is irregular.
- Once the mosquito decides that it is poised to balance the proboscis while pushing it into the skin, it starts to apply axial thrusts while balancing the proboscis against bending. This process continues for several seconds. Significant penetration has not occurred as evidenced by a lack of a small loop of the labium near the mouth. The fascicle is inside the labium completely. This is shown in figure 5(*B*).
- Once the mosquito succeeds in pushing down the fascicle further into the skin after repeated attempts in one promising spot, as evidenced by a small departure of the labium near the mouth with fascicle exposed, it starts to push the fascicle down by folding its front legs gradually, while moving the head back and forth to avoid proboscis buckling and complete the penetration process. The labium loop that is formed near the mouth exposes a small portion of the fascicle due to its inverted gutter-like structure [18], but supports the fascicle at the skin end completely.
- During this early penetration stage, the small labium loop is seen to appear and disappear at about the same frequency (15 Hz), indicating that the mosquito is axially pushing and withdrawing the fascicle repeatedly and attempting to progressively penetrate further into the skin. As penetration proceeds further, the free length of fascicle under compressive load decreases and the labium fold increases in length proportionately. Under the skin, the lateral support provided by skin tissue prevents bucking due to compressive force. Thus, the fascicle becomes progressively stable with increasing penetration. This is evidenced by a decrease in the frequency of head lateral movement from the initial 15–17 Hz to about 6 Hz towards the middle to end of the penetration process. The amplitude of axial movement increases, as evident in another published video of the penetration process [32]. The vertical thrusting is not visible. However, the effect of thrust causing lateral instability is visible through the lateral movement of the proboscis and the tilting of the head and makes it possible to make these frequency estimates. The sequence of penetration into the skin is represented in figure 6.

In order to validate our visual observations under a high-speed camera and subsequently analyzing the time sequence frame by frame to arrive at the above mentioned observations and measurements, we compared our observations with an electrical impedance measurement technique for studying the

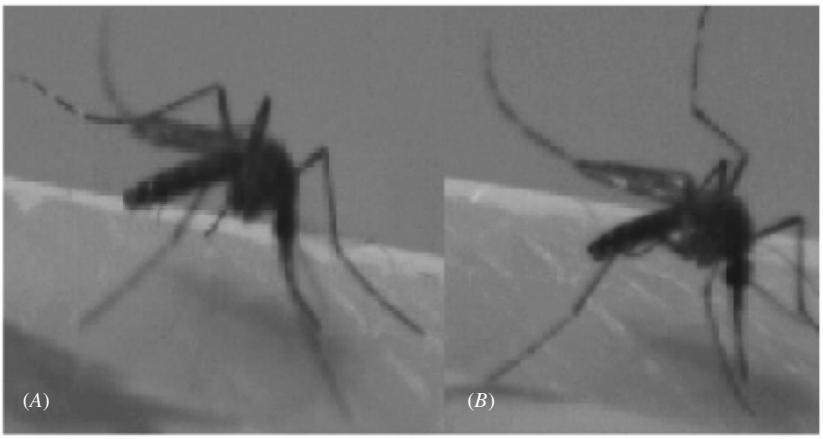

Figure 5. (*A*) Unsuccessful attempt; (*B*) successful anchoring of the proboscis without bending.

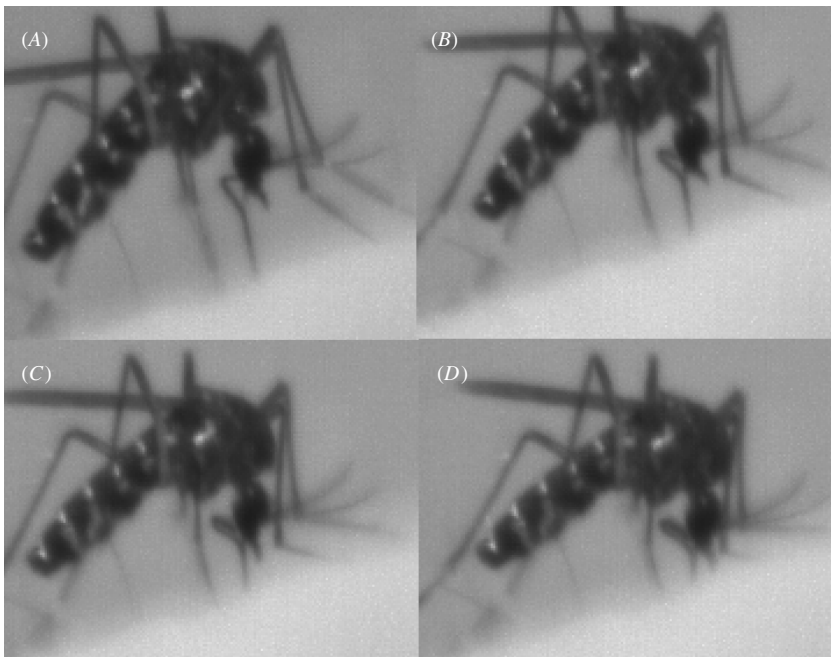

Figure 6. Mosquito skin penetration sequence from HSV filming.

biting process that was presented by Kashin [33]. He used the mosquito to close the electrical circuit between a wire mesh and a live mouse. Electrical conduction is achieved only when there is penetration. Using the electrical impedance measurements with *aedes ageypti*, the process of biting was described in detail by Kashin [35]. The electrical impedance is highest before penetration occurs as the outer layer of the skin has the highest resistance. Once penetration occurs, the resistance drops. After reaching sufficient depth where the fascicle contacts the blood stream in a capillary or a pool of blood under the skin caused by hemorrhage, the resistance drops to its lowest level. The probing process displays small drops in resistance and recovery back to full value, and the probing process taking place at the rate of approximately 2 per second, although it is irregular. Once the mosquito is still (in biting attitude), but engorgement has not occurred, the frequency becomes regular, and the signal fluctuates at 7 Hz. We explain this variation as primarily due to the fascicle entering the skin, and the mosquito withdrawing it due to buckling initiation. Once engorgement is observed, they report a signal frequency of about 15 Hz. They attribute it to the closing and opening of the thorax valve. In addition, excursions of the electric signal at low frequencies (about 5 Hz) but varying amplitudes were reported. Larger excursions were attributed to pool feeding and short excursions were attributed to capillary feeding. In the case of pool feeding, the mosquito creates a hemorrhage and feeds on the blood pool created whereas in capillary feeding it directly connects into a capillary and the blood is driven under pressure into the mosquito and hence this process is faster [35]. In our observation, we found different mosquitoes taking different times. In one case, a mosquito barely introduced its fascicle into the skin and perhaps hit a capillary directly and engorged very quickly. In other cases, such as the one shown in the video in this paper, the mosquito had to push all the way before reaching a pool of blood and took the longest time. Our observations are totally consistent with prior published results [35]. We have established a high-speed video image of the mosquito biting process that can be used to develop mechanics models.

We are concerned with the process of penetration starting with the completion of probing and moving (figure 5(*B*)) to penetration of the fascicle into the skin (figure 6(*A*)). In our work, we are primarily concerned with the initial penetration mechanics to establish the maximum force required for penetration and the set of movements at the tip of the fascicle necessary to accomplish initial penetration (figures 5(*B*) and 6(*A*)). The low-frequency axial thrusting and folding of the leg to push the fascicle into the skin is not considered in this work.

We hypothesize that the buckling initiation is sensed by the mosquito and it reduces the force, reorients and repositions the head slightly and attempts again. This phenomenon is seen as lateral head movement as the axial movement is very small and cannot be seen until actual penetration is initiated. Further, the tilting of the head during the course of penetration, typically 10–20° to the vertical, is modeled as a non-conservative follower force component of the axial compressive force to study the importance of such a force in the penetration process. This may have significance in increasing the bucking load for successful penetration, particularly after initially anchoring the fascicle. The lateral support provided by the labium is another factor influencing the bucking load. In order to understand the effects of non-conservative load application and the influence of labium support, we propose a mathematical model that takes into account both these effects, describes the penetration process and assesses the significance of lateral support and non-conservative forces.

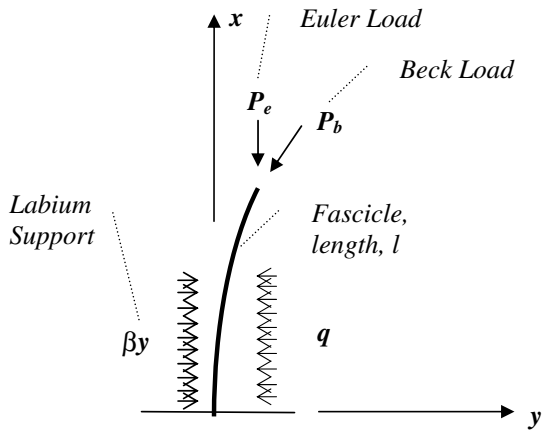

Figure 7. Forces on a fascicle during an attempt to penetrate the skin.

3. Theory

Figure 7 shows a schematic of a fascicle that has just contacted the skin and being pushed down by the mosquito's head. The force applied by the mosquito at every axial thrust and a short time following the thrust can be resolved into two components, namely, the Euler load, represented by P_e and a non-conservative load component tangential to the tip of the fascicle at the mouth, represented by P_b, also known as Beck load. The fascicle is supported laterally by the labium. The labium is modeled as an elastic foundation that opposes the lateral motion of the fascicle. q is the distributed force per unit length, and β is the foundation modulus (force per unit deflection per unit length).

Following the analysis of a beam initially straight, resting on an elastic foundation, subjected to an axial compressive load of the Euler type (P_e), the equation of equilibrium of an infinitesimal axial element can be written as [22]

$$EI\frac{\mathrm{d}^4y}{\mathrm{d}x^4} + P_e\frac{\mathrm{d}^2y}{\mathrm{d}x^2} + \beta y = q. \tag{1}$$

Applying D'Alembert's principle we can replace the lateral load q by the inertial force, and adding the non-conservative component of the applied force, P_b, in the initial straight configuration [22–25], we can write the governing equation of motion for a column that is subjected to both Euler and Beck loads simultaneously with lateral elastic foundation support as [26]

$$\frac{\partial^4 y}{\partial x^4} + \left(\frac{P_e + P_b}{EI}\right)\frac{\partial^2 y}{\partial x^2} + \frac{m}{EI}\frac{\partial^2 y}{\partial t^2} + \frac{\beta}{EI}y = 0 \tag{2}$$

where m is the mass per unit length of the fascicle, E is the elastic modulus of the chitin material that the fascicle is made of and I is the moment of inertia of the cross section of the fascicle. The boundary conditions are

$$\begin{aligned} y(0,t) &= 0 \\ y'(0,t) &= 0 \\ y''(l,t) &= 0 \\ y'''(l,t) + \frac{P_e}{EI}y'(l,t) &= 0 \end{aligned} \tag{3}$$

where l is the length of the fascicle.

Let ξ be the non-dimensional axial coordinate so that $\xi = x/l$, and introduce the following non-dimensional terms:

$$\begin{aligned} k^2 &= \frac{P_e + P_b}{EI}l^2 \\ \lambda_e &= \frac{P_e}{EI}l^2 \\ \lambda_b &= \frac{P_b}{EI}l^2 \\ k^2 &= \lambda_e + \lambda_b \\ a &= \frac{ml^4}{EI} \\ \alpha &= \frac{\beta l^4}{EI}. \end{aligned} \tag{4}$$

The governing equation of motion (2) in terms of these non-dimensional quantities can be written as

$$\frac{\partial^4 y}{\partial \xi^4} + k^4\frac{\partial^2 y}{\partial \xi^2} + a\frac{\partial^2 y}{\partial t^2} + \alpha y = 0. \tag{5}$$

Let $y = W(\xi)\,\mathrm{e}^{\mathrm{i}\omega t}$ be the solution to the above equation. Substituting, we obtain

$$\frac{\mathrm{d}^4 W}{\mathrm{d}\xi^4} + k^2\frac{\mathrm{d}^2 W}{\mathrm{d}\xi^2} - (a\omega^2 - \alpha)W = 0. \tag{6}$$

Assuming the general solution to (6) as

$$W(\xi) = A\cosh\lambda_1\xi + B\sinh\lambda_1\xi + C\cos\lambda_2\xi + D\sin\lambda_2\xi \tag{7}$$

and substituting into (6), we obtain two characteristic equations. The characteristic equation for the sine and cosine terms is given by

$$\lambda_2^4 - \lambda_2^2k^2 - (a\omega^2 - \alpha) = 0. \tag{8}$$

And the roots are

$$\lambda_2^2 = \frac{k^2 + \sqrt{k^4 + 4(a\omega^2 - \alpha)}}{2}. \tag{9}$$

The characteristic equation for the hyperbolic terms is given by

$$\lambda_1^4 + \lambda_1^2k^2 - (a\omega^2 - \alpha) = 0. \tag{10}$$

And the roots are

$$\lambda_1^2 = \frac{-k^2 + \sqrt{k^4 + 4(a\omega^2 - \alpha)}}{2}. \tag{11}$$

Substituting the assumed solution (7) into boundary conditions (3) and simplifying [26], we obtain a final transcendental equation to solve

$$\begin{aligned} &\lambda_1^2\lambda_e + \lambda_1^4 + \lambda_2^4 - \lambda_2^2\lambda_e \\ &\quad + \left[-\lambda_1^3\lambda_2 + \lambda_1\lambda_2^3 - 2(\lambda_1\lambda_2\lambda_e)\right](\sinh\lambda_1\sin\lambda_2) \\ &\quad + \left[2\left(\lambda_1^2\lambda_2^2\right) + \lambda_e\left(-\lambda_1^2 + \lambda_2^2\right)\right](\cosh\lambda_1\cos\lambda_2) = 0. \end{aligned} \tag{12}$$

In order to verify the derivation, three classical degenerate cases were deduced from this general result.

Case 1: pure Beck (non-conservative load) load with no Euler load or elastic foundation

Setting $\alpha = 0$, and $\lambda_\varepsilon = 0$, equation (12) becomes

$$\lambda_1^4 + \lambda_2^4 + \left(-\lambda_1^3\lambda_2 + \lambda_1\lambda_2^3\right)(\sinh\lambda_1 \sin\lambda_2) + 2\left(\lambda_1^2\lambda_2^2\right)(\cosh\lambda_1 \cos\lambda_2) = 0. \quad (13)$$

Using equations (9) and (11), we can reduce the above equation to the familiar form of the transcendental equation for a pure Beck loading case [22–25] as

$$k^4 + 2a\omega^2 + k^2\sqrt{a\omega^2}(\sinh\lambda_1 \sin\lambda_2) + 2a\omega^2(\cosh\lambda_1 \cos\lambda_2) = 0. \quad (14)$$

Case 2: the same as case 1 without Beck load.

Substituting $k = 0$ in (14), we obtain

$$1 + \cosh\lambda_1 \cos\lambda_2 = 0. \quad (15)$$

This is the familiar case of a bar in free bending vibration [22]. Thus the equations describe the degenerate cases correctly.

4. Results

Equation (13) was solved in Matlab® numerically for two distinct cases of instabilities, as defined by Rao and Singh [24], namely divergence and flutter instabilities. Rao and Singh [27] showed that the presence of a non-conservative Beck force can increase the Euler buckling load of columns by a factor of 3.5 for a cantilever beam. Since we hypothesized that the mosquito may be applying some nonconservative force by tilting the head, we present our results in the general framework of Rao and Singh [24] to assess the importance of Beck loading. We follow the method described in [24] for the solution of equation (13) and plot the results consistent with Rao and Singh [24] for comparison. For a given value of Beck load, the value of Euler load is increased until the fundamental frequency becomes zero. This determines the divergence instability critical load pairs. For a given value of Euler load, the Beck load is increased until the first two resonant frequencies coincide, defining flutter instability [24]. The coalescing point defines a pair of critical values for Beck and Euler loads. These critical load pairs are plotted. However, we evaluated the equation for different values of foundation stiffness by varying the parameter α, to observe the effect on the critical load pairs. Figure 8 shows the flutter and divergence critical pairs with $\alpha = 0$, i.e. no elastic foundation, with solid square points representing flutter instability, and solid circles representing divergence instability with $\alpha = 0$. Starting at zero Beck load, and increasing that load to just below a value of 0.7, the Euler critical buckling load is raised by a factor of almost 3 before divergence instability occurs. This result is consistent with the results obtained by Rao and Singh [26].

Flutter generally occurs at or near the natural frequency of the structure [37]. We calculated the first natural frequency of the fascicle with the best available properties. The bending vibration natural frequency for a fixed-free beam is given by [28]

$$f = 1.875\sqrt{\frac{EI}{mL^4}} \quad (16)$$

where f is the natural frequency of the beam, E is the elastic modulus, I is the moment of inertia of cross section, m is the mass per unit length of the beam and L is the length of the beam. The elastic modulus E of chitin polymer that the fascicle is made of is between 10 and 200 GPa [29], and the density of chitin is about 1500 kg m^{-3}. Assuming the elastic modulus to be 20 GPa, which is in the range of values possible [29], the dimensions of a fascicle to be 40 μm OD, 20 μm ID, and 2 mm in length, the natural frequency computed using equation (16) is 36 kHz. The mosquito increases the load from zero to the maximum, until it detects instability, whereby it reduces the load, repositions the geometry and tries again. In every case, for slowly increasing loads (at most 17 Hz observed frequencies of movement), the analysis shows that the divergence instability is met before reaching the flutter curve. Hence, divergence instability is considered the physically limiting case for a mosquito fascicle under compression and flutter may be suppressed and may not be important. Flutter suppression has been observed in other composite systems such as carbon nanotubes embedded in a moderately stiff Winkler foundation [36]. We have plotted the divergence instability criteria for different foundation stiffness and Beck loads. Figure 8 shows a plot of the effect of non-zero α on the first divergence curve. As α is increased, the curves move toward higher values of Euler load. Increasing α does not shift the flutter curve. It simply raises the frequency of coalescence but the critical Beck/Euler pairs are not affected.

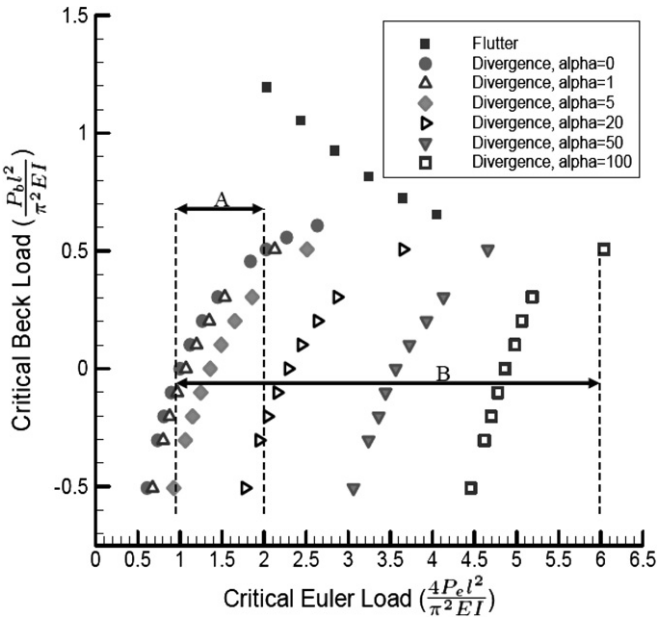

Figure 8. Critical load pairs for non-zero lateral support and Beck load.

5. Discussion

Our final result from the analytical studies is summarized in figure 8. The distance marked A shows an increase in Euler load from 1 to 2, primarily through the application of Beck load of about 0.5, without significant lateral support stiffness. Thus, application of nonconservative force in and of itself increases the bucking load. As the foundation stiffness is increased from $\alpha = 0$ to $\alpha = 100$, the distance marked B shows an increase in

Euler load from 1 to 6 for the same non-conservative load of 0.5. If the nonconservative load is completely eliminated, still the increase in buckling load is from 1 to about 5 for this case of $\alpha = 100$. It is observed that with no foundation stiffness, the maximum increase in Euler load can be from 1 to 3.5 for a value of Beck load about 0.7, before the flutter instability curve is encountered, and represents the theoretical maximum for that case.

Thus, a mosquito is balancing the fascicle during penetration against divergence instability by the back and forth head movement at 17 Hz in the beginning of the probing process. As penetration occurs, the shortening of the free length of the fascicle and the associated support of the fascicle underneath the skin increase the Euler load (or the threshold of divergence instability) thereby necessitating a lower frequency of head movement. Furthermore, the lateral support stiffness has a higher potential to support the fascicle and increase the buckling load relative to the application of nonconservative load. It can be concluded that the lateral support is critical in enabling the mosquito to penetrate the skin. The critical load for a fixed-free beam subjected to axial compression is given by [22]

$$P_{cr} = \frac{\pi^2 EI}{4L^2}. \tag{17}$$

Substituting the values for E, I and L, for a fascicle, we obtain the critical load. While the diameters and length of the fascicle were determined through direct measurements under the SEM, the elastic modulus of chitin was estimated from published values. The value of elastic modulus for pure chitin has been reported to be spread over a wide range (10–200 GPa) [29]. Specific determinations of the elastic modulus of chitin have been reported. The elastic modulus of crystalline chitin was reported to be 41 GPa by Nishino *et al* [38]. Maeda *et al* [39] reported a value of 6.2 GPa in the dry state and a severe reduction in modulus as much as one fiftieth when measured in the wet state for chitin rods. Wan *et al* [40] report a value of modulus of about 5 GPa. Thus, a value of 20 GPa for elastic modulus provides an upper bound estimate of the buckling critical load as 3.0 mN. Roxhed *et al* [34] reported a measurement of 10 mN as the lowest insertion force for a microneedle by using an ultra sharp cylindrical needle with a tip radius of 0.1 μm, compared to a minimum force of 100 mN for a tip radius of 75 μm by Davis *et al* [15]. Thus, the fascicle alone, with an upper bound buckling critical load of about 3 mN, is incapable of penetrating the skin by directly pushing into the skin. From the mathematical model results (figure 8), if the mosquito applies a non-conservative force of 0.5 (non-dimensionalized), and the labium offers a lateral support coefficient of $\alpha = 100$ (non-dimensionalized), there is a 6× increase in the buckling load of the fascicle to 18 mN. If Beck load is not applied, then the lateral support provides a 5× increase in buckling load, 15 mN. In either case, the force exceeds the minimum required force of 10 mN reported for an ultra sharp needle [34]. Thus, it is understandable that the mosquito makes several attempts before piercing the skin successfully as it is barely able to apply the minimum necessary force and hence it has to look for the right spot. Further, the mosquito needs to orient the proboscis such a way that initial buckling is prevented, while applying some nonconservative force to counter divergence instability, thereby increasing the bucking load. It is known that the effect of increasing sharpness of the tip is to decrease the insertion force without buckling [34, 15]. Thus, it is concluded that the lateral support of the labium is essential for fascicle penetration into the skin and is more important than the Beck loading. Lateral support alone provides an increase in buckling load sufficient to penetrate the skin for ultra sharp tips. The effect of Beck loading, in addition to the lateral support, further increases the buckling load by 20% and further facilitates penetration, but is not always necessary. In order to understand the magnitude of the non-dimensional parameters, α, and non-dimensionalized Beck loading, we have computed the load values for interpretation. For $\alpha = 100$, for the fascicle properties used in this study, we get a foundation stiffness of 60 N m^{-1}. For a lateral deflection of the fascicle of 100 μm at the center, the foundation applied force is 6.0 mN. Considering that the mosquito applies an axial Euler load of 18 mN and a Beck load of 0.4 mN, the foundation applied force of 6.0 mN is of the same order of magnitude, which is possible and realistic.

It is quite challenging to produce experimental observations to conclusively establish the importance of labium support for successful penetration into the skin. Fortunately, this work has been done and reported decades ago in a paper by Jones and Plitt [30]. In their work, they systematically removed various appendages from mosquitoes and observed their feeding behavior. First, they cut off the tip of the labella (outer sheath tip) along with the tip of the fascicle. In other words, they cut the proboscis at the tip right across. They observed that the mosquitoes would position themselves correctly for feeding, but when they shifted their weight to penetrate the skin, the proboscis simply slid under their bodies, i.e. buckled every time. This is partly due to the fact that the cut makes the fascicle into a cylinder with a flat, blunt end. Hence it cannot penetrate the skin and the applied forces simply reached the buckling load in every attempt. This establishes the importance of tip sharpness on the penetration force. In another experiment, they cut the labella (tip of the outer sheath, labium) off, but not the fascicle. The fascicle tip was exposed at the tip (similar to figure 2, but the labella was cut off). Penetration was not achieved. More importantly, the females did not even probe as their sensory organs located on the labella were lost. If the mosquitoes did attempt to penetrate, the proboscis simply buckled. Finally, they desheathed the fascicle using the loop method in which the fascicle was exposed outside the labium, but the labium was not cut off, but simply moved out of the way temporarily. The mosquitoes with exposed fascicles were not able to penetrate as the fascicle buckled every time. When they released the labium and resheathed the fascicle, the same mosquitoes had no problem penetrating the skin again. This careful experimentation and observations offer the strongest validation for the model results and the mechanism by which a mosquito is able to use its slender fascicle and insert it into the skin.

6. Conclusions

The feeding behavior of the female mosquito has been studied both experimentally and analytically with the objective of explaining the process in mechanistic terms. To the best of our knowledge, this represents the first such attempt. The anatomical details were presented through SEM pictures and the dynamics of mosquito fascicle penetration has been presented through high-speed video imaging at high magnification. It has been observed that the mosquito moves its head back and forth, at a frequency starting from 15–17 Hz and gradually reducing to about 6 Hz during the insertion process. The critical buckling load for a typical fascicle is very low (∼3 mN) and not sufficient to penetrate the skin. However, the fascicle is laterally supported throughout the process by the labium and it was hypothesized that the mosquito applies some non-conservative Beck force component during downward movement. A mathematical model to assess the importance of the labium support and possible non-conservative force application was developed and solved numerically. The presence of lateral support, together with a Beck load component, increases the Euler buckling load for divergence instability by a factor of 6 (∼18 mN). Without the Beck load, the increase is by a factor of 5. The lowest known penetration force for an ultra sharp cylindrical microneedle is 10 mN. Thus, the lateral support of the labium with or without Beck load helps the mosquito reach above this threshold to penetrate the skin. The lateral support of the labium is critical. Beck loading provides an additional mechanism to increase the load by 20%. The model results showing the importance of lateral support have been validated with well established experimental results on mosquito feeding behavior. The mosquito fascicle-labium system, or the proboscis, is barely optimal for penetrating into the skin for blood drawing. Thus, careful attention must be paid to the dimensions and structure of the proboscis and the dynamics of a mosquito bite. Sub-micrometer tip radii observed in the SEM pictures and the tip reinforcement ridge both favor lower penetration force. An ultra sharp polymeric needle with some form of lateral support can penetrate the skin painlessly as the size can be reduced to the dimensions of a fascicle. While these dimensions are achievable using silicon micromachining, brittle fracture of the tip *in vivo* will be a deterrent to miniaturizing silicon needles further. Further work to quantitatively determine the lateral support properties, the effect of salivation, friction between the fascicle and labium, and the use of realistic skin constitutive models and material models for the fascicle and labium in a numerical simulation of the penetration process is planned.

Acknowledgments

The financial support from the National Science Foundation through grant number CMS 0402857 is acknowledged. We would also like to acknowledge the support of Dr Charles Apperson, Professor, Entomology, NC State University, for his assistance with the experiments, and Dr Jay Tu, Professor, Mechanical and Aerospace Engineering, NC State University for his suggestions.

References

[1] Oki A, Takai M, Ogawa H, Takamura Y, Fukasawa T, Kikuchi J, Ito Y, Ichiki T and Horiike Y 2003 Healthcare chip for checking health condition from analysis of trace blood collected by painless needle *Japan. J. Appl. Phys.* **42** 3722–27

[2] Ogawa H, Nagai M, Kikuchi J and Horiike Y 2003 Blood painless collection system equipping detection functions for search of vein *7th Int. Conf. Miniaturized Chemical and Biochemical Analysis Systems (741–3 Squaw Valley, CA, USA)*

[3] Henry S, McAllister D V, Allen M G and Prausnitz M R 1998 Micromachined needles for the transdermal delivery of drugs *Proc. IEEE Micro Electro Mechanical Systems, MEMS'98 (Heidelberg, Germany, Jan. 25–29* pp 494–8

[4] Oka K, Aoyagi S, Arai Y, Isono Y, Hashiguchi G and Fujita H 2002 Fabrication of a micro needle for trace blood test *Sensors Actuators* A **97–98** 478–85

[5] Khumpuang S, Horade M, Fujioka K and Sugiyama S 2007 Geometrical strengthening and tip-sharpening of a microneedle array fabricated by x-ray lithography *Microsyst. Technol.* **13** 209–14

[6] Gill H S and Prausnitz M R 2007 Coated microneedles for transdermal delivery *J. Control. Release* **117** 227–37

[7] Nordquist L, Roxhed N, Griss P and Stemme G 2007 Novel microneedle patches for active insulin delivery are efficient in maintaining glycaemic control: an initial comparison with subcutaneous administration *Pharm. Res.* **24** 1381–8

[8] Zimmermann S, Fienbork D, Stoeber B, Flounders A W and Liepmann D 2003 Microneedle-based glucose monitor fabricated on a wafer-level using in-device enzyme immobilization *TRANSDUCERS '03: 12th Int. Conf. Solid State Sensors, Actuators and Microsystems (Boston, MA, June 8–12)* pp 99–102

[9] Gattiker G E, Kaler K V I S and Mintchev M P 2005 Electronic mosquito: designing a semi-invasive microsystem for blood sampling, analysis and drug delivery applications *Microsyst. Technol.* **12** 44–51

[10] Tsuchiya K, Nakanishi N, Uetsuji Y and Nakamachi E 2005 Development of blood extraction system for health monitoring system *Biomed. Microdev.* **7:4** 347–53

[11] Han M, Hyun D H, Park H H, Lee S S, Kim C H and Kim C G 2007 A novel fabrication process for out-of-plane microneedle sheets of biocompatible polymer *Micromech. Microeng.* **17** 1184–91

[12] Martanto W, Moore J S, Kashlan O, Kamath R, Wang P M, O'Neal J M and Prausnitz M R 2006 Microinfusion using hollow microneedles *Pharm. Res.* **23** 1

[13] Yang M and Zahn J 2004 Microneedle insertion force reduction using vibratory actuation *Biomed. Microdev.* **6** 177–82

[14] Newton A, Lal A and Chen X 2003 Ultrasonically driven microneedles *NNUN REU Program at Cornell University* pp 34–35

[15] Davis S P, Landis B J and Adams Z H 2004 Insertion of microneedles into skin: measurement and prediction of insertion force and needle fracture force *J. Biomech.* **37** 1155–63

[16] Clements A N 1992 *The Biology of Mosquitoes* (London: Chapman and Hall)

[17] Daniel T L and Kingsolver J G 1983 Feeding strategy and the mechanics of blood sucking in insects *J. Theor. Biol.* **105** 661–72

[18] Jones J C 1978 The feeding behavior of mosquitoes *Sci. Am.* (June) 138–48

[19] Griffiths R B and Gordon R M 1952 An apparatus which enables the process of feeding by mosquitoes to be observed in tissues of a live rodent, together with an

account of the ejection of saliva and its significance in malaria *Ann. Trop. Med. Parasit.* **46** 311–9
[20] Ribeiro J M C 1984 Role of mosquito saliva in blood vessel location *J. Exp. Biol.* **108** 1–7
[21] Swaminathan V 2006 Mechanics of a mosquito bite *MS Thesis* Department of Mechanical and Aerospace Engineering, NC State University, Raleigh, NC
[22] Timoshenko S 1961 *Theory of Elastic Stability* (New York: McGraw-Hill)
[23] Beck V M 1952 Die knicklast des einseitig eingespannten, tangential gedrůckten stabes *Z. Angew. Math. Phys.* **3** 225–8
[24] Rao G V and Singh G 2001 Revisit to the stability of a uniform cantilever column subjected to Euler and Beck loads—effect of realistic follower forces *Indian J. Eng. Mater. Sci.* **8** 123–8
[25] Celep Z 1977 On the vibration and stability of Beck's column subjected to vertical and follower forces *Z. Angew. Math. Mech.* **57** 555–7
[26] Barham O M 2007 A mathematical model for the mechanics of a mosquito bite with applications to microneedle design *MS Thesis* Department of Mechanical and Aerospace Engineering, NC State University, Raleigh, NC
[27] Rao G V and Singh G 2001 A smart structures concept for the buckling load enhancement of columns *Smart Mater. Struct.* **10** 843–5
[28] Meirovich L 1967 *Analytical Methods in Vibrations* (New York: Macmillan)
[29] Vincent J F V and Wegst U G K 2004 Design and mechanical properties of insect cuticle *Arthropod Struct. Dev.* **33** 187–99
[30] Jones J C and Plitt D R 1973 Blood-feeding behavior of adult *Aedes Aegypti* mosquitoes *Biol. Bull.* **145** 127–39
[31] Wick C, Benedict J T and Veillex R F (ed) 1984 Stamping press operations *Tool and Manufacturing Engineers Handbook: Volume II. Forming* (Dearborn, MI: Society of Manufacturing Engineers) chapter 4, pp 4–9
[32] Video footage from http://www.naturefootage.com/stockfootage/Mosquito
[33] Kashin P and Wakeley H G 1965 An insect "Bitometer" *Nature* **208** 462–4
[34] Roxhed N, Gasser C T and Griss P 2007 Penetration-enhanced ultrasharp microneedles and prediction on skin interaction for efficient transdermal drug delivery *J. Microelectromech. Syst.* **16** 1429–40
[35] Kashin P 1966 Electronic recording of the mosquito bite *J. Insect Physiol.* **12** 281–6
[36] Yoon J, Ru C Q and Mioduchowski 2006 Flow-induced flutter instability of cantilever carbon nanotubes *Int. J. Solids Struct.* **43** 3337–49
[37] Hoey R G 2003 Flutter excitation, information summary *NASA, IS-97/08-DFRC-F1* (Nov 19)
[38] Nishino T, Matsui R and Nakamae K 1999 Elastic modulus of the crystalline regions of chitin and chitosan *J. Polym. Sci.* B **37** 1191–6
[39] Maeda M, Inoue Y, Iwase H and Kifune K 1984 Characteristics of chitin for orthopedic use *Chitin, Chitosan and Related Enzymes* ed P Zikakis (New York: Academic) pp 411–5
[40] Wan A C A, Eugene I and Hastings G W 1997 Hydroxyapatite modified chitin as potential hard tissue substitute material *J. Biomed Mater. Res. (Appl. Biomater.)* **38** 235–41